# Estimates of the quantum Fisher information in the $S = 1$ antiferromagnetic Heisenberg spin chain with uniaxial anisotropy

J. Lambert* and E. S. Sørensen†
*Department of Physics & Astronomy, McMaster University, 1280 Main St. W., Hamilton, ON, Canada L8S 4M1*

(Received 22 October 2018; revised manuscript received 19 December 2018; published 9 January 2019)

The quantum Fisher information is of considerable interest not only for quantum metrology but also because it is a useful entanglement measure for finite temperature mixed states. In particular, it estimates the degree to which multipartite entanglement is present. Recent results have related the quantum Fisher information to experimentally measurable probes. While in principle possible, a direct evaluation of the quantum Fisher information at finite temperatures is technically challenging and here we show that a simple estimate can be obtained for materials where the single-mode approximation is valid. We focus on the $S = 1$ antiferromagnetic Heisenberg model with uniaxial anisotropy. Quantum Monte Carlo techniques are used to determine low-temperature correlations from which the quantum Fisher information can be estimated within the single-mode approximation. The quantum Fisher information is compared to the quantum variance for the staggered magnetization operators in the transverse direction and inequalities between the quantum Fisher information, the quantum variance, and the full variance are discussed. Both the quantum and full variance as well as the quantum Fisher information are examined at finite temperatures above the isotropic point and at the quantum critical point for the Haldane-Néel transition. A finite size scaling study of the quantum Fisher information is performed at the quantum critical point and used to confirm the Ising nature of the Haldane-Néel transition.

DOI: 10.1103/PhysRevB.99.045117

## I. INTRODUCTION

The quantum Fisher information (QFI), $F_Q$, is often studied in quantum metrology [1–6]. There, one considers unitary dynamics $U = \exp(-i\hat{O}\theta)$ and the phase estimation sensitivity is then limited by the Cramér-Rao bound $(\Delta\theta)^2 \geqslant 1/F_Q[\hat{O}]$ for *any* measurement. From a condensed-matter perspective, the quantum Fisher information is particularly interesting since it can be used to estimate multipartite entanglement even at finite temperatures since $F_Q/N > m$ with $m$ a divisor of $N$ signals $(m+1)$-partite entanglement [4,6–8]. Significant progress in the understanding of, in particular, bipartite, entanglement in quantum many-body systems has been made [9–11]. More recently, a host of techniques have been developed to efficiently quantify multipartite entanglement in quantum many-body systems. (For a review of entanglement witnesses, see [12–15]). For our purpose we will take the definition of multipartite entanglement to be the natural generalization of bipartite entanglement. Namely, consider an $N$-body quantum state $|\psi_N\rangle$. Now imagine expressing this state as a product of $m$ states each containing $N_m$ particles $|\psi_N\rangle = \bigotimes_{i=0}^{m} |\phi_i\rangle$. A $k$-partite entangled state is one for which the largest constituent state $\phi_i$ contains $N_i = k$ particles, and cannot be further decomposed. It's clear that one can recover from this the usual definition of bipartite entanglement. Measuring bipartite entanglement is often achieved through the von Neumann entropy, $S_A = -\mathrm{Tr}(\hat{\rho_A} \ln \hat{\rho_A})$, where $\rho_A$ is the partial trace of the full density matrix $\hat{\rho}$. This measure determines the amount of entanglement between the subsystem $A$ and its complement, $B$. It does not, however, tell us how many particles are entangled in the state. It is in this respect that the QFI differs from the von Neumann entropy in that the QFI allows for measurments of the precise number of particles that are in the most entangled factor state. Ideally, for the study of multipartite entanglement, one would like to use techniques that do not rely on a particular knowledge of the density matrix, as these are the techniques most easily connected to experiment and the QFI seems well suited for this purpose.

Quantifying multipartite entanglement is well motivated by the study of quantum criticality, particularly in systems with phases that are topological in nature. These phases are not characterized by a local order parameter, making the detection of these phases challenging. By measuring the multipartite entanglement through the QFI, progress has been made in exploring the phase diagram of the Kitaev model, which exhibits a topological phase [16]. The QFI has also found application in exploring the non-Markovian limit of open quantum systems [17]. In general, multipartite entanglement must also play a role in isolated quantum dynamics, where systems appear to locally thermalize. Experimental work in [18] has established this connection, and it is therefore reasonable to expect that the QFI will play a role in examining questions of thermalization as well.

The QFI has long been known as a monotonic multipartite entanglement measure [4,6–8], but only recently has it been connected to the dynamic structure factor which is easily accessed by experimental probes such as neutron scattering [19]. This has led to the studies of the QFI and multipartite entanglement in the Kitaev chain [16], quantum Ising

*lambej3@mcmaster.ca
†sorensen@mcmaster.ca

 

chain [19], XY spin chain [20], XXZ spin chain [21], and Lipkin-Meshkov-Glick model [22,23]. In order to access the QFI these studies all rely on the exact solvability of the models considered and from a numerical perspective, accessing the Fisher information can be challenging in particular at finite temperature for realistic nonintegrable quantum many-body models. Experimental efforts have also yielded results in estimating the entanglement through the QFI using collections of local measurements, which circumvent the need for full knowledge of the dynamic structure factor [24]. Here we show that a simple estimate of the QFI, $F_Q^{\mathrm{SMA}}$, can be obtained by using the single-mode approximation (SMA) which allows the QFI to be calculated directly from the equal-time structure factor. The quantum variance (QV) has been established as a lower and upper bound for $F_Q$, $4\langle\delta^2\hat{O}\rangle_Q \leqslant F_Q \leqslant 12\langle\delta^2\hat{O}\rangle_Q$ [25], and at the same time a different upper bound is given by the full variance $F_Q \leqslant 4\langle\delta^2\hat{O}\rangle$ [6]. This then serves as a rigorous check on the validity of the SMA calculations.

We focus on the $S = 1$ antiferromagnetic (AFM) Heisenberg model with uniaxial anisotropy,

$$\hat{H} = J\sum_i \left[\boldsymbol{S}_i \cdot \boldsymbol{S}_{i+1} + D\left(S_i^z\right)^2\right], \tag{1}$$

where $D$ is the uniaxial anisotropy and we shall take $J = 1$ throughout. At $D = 0$ this model displays the celebrated Haldane gap at $k = \pi$ of $\Delta \sim 0.41J$ and it is quite well established [26,27] that the single-mode approximation works very well around $k = \pi$ for moderate values of $D$. We perform stochastic series expansion [28–30] (SSE) quantum Monte Carlo simulations to evaluate low-temperature equal-time correlations, from which $F_Q^{\mathrm{SMA}}$ is obtained, as well as finite temperature calculations to determine the quantum and full variance. This demonstrates the presence of significant multipartite entanglement even at the isotropic point $D = 0$.

The layout of this paper is as follows. In Sec. II we introduce some of the key properties of the QFI and QV (Sec. II A). We then introduce the single-mode approximation (Sec. II B) and its application to the $S = 1$ AFM Heisenberg model. Then in Sec. III we present SSE results for the system QV and the QFI at the isotropic point as well as for a range of values $D < 0$ toward the quantum critical point before turning to our conclusions in Sec. IV.

## II. TECHNIQUES

### A. QFI and QV

The quantum Fisher information is one possible generalization of the classical Fisher information, which quantifies the distinguishability of a family of distributions parametrized by one (or possibly several) parameters $\theta$ [31,32]. The quantum generalization of this quantifies the distinguishability of a family of quantum states defined by

$$\rho(\theta) = e^{-i\theta\hat{O}}\rho e^{i\theta\hat{O}}, \tag{2}$$

where $\hat{O} = \sum_r \hat{O}_r^\alpha$ is a sum over local operators. In particular, the QFI can be thought of as the statistical speed related to the rate of change of the Bures distance, which is a metric on the space of density matrices [33]. For a density matrix that in its eigenbasis is given by

$$\rho = \sum_\lambda p_\lambda |\lambda\rangle\langle\lambda|, \tag{3}$$

the QFI is given by

$$F_Q = 2\sum_{\lambda,\lambda'} \frac{(p_\lambda - p_{\lambda'})^2}{p_\lambda + p_{\lambda'}} |\langle\lambda'|\hat{O}|\lambda\rangle|^2. \tag{4}$$

The relationship between the QFI and the multipartite entanglement has been well established in [4–8]. In particular, for a QFI density:

$$f_Q \equiv F_Q/N > m, \tag{5}$$

where $m$ is a divisor of $N$, the system is $(m+1)$-partite entangled. The QFI thus increases monotonically with the entanglement. One of the most appealing features of the QFI is that it is defined for mixed states, allowing one to determine the entanglement content of a state at finite temperature. Recent work [19] has connected the QFI density to the dynamic structure factor,

$$f_Q(k) = \frac{2}{N^d\pi}\int_{-\infty}^{\infty} d\omega \tanh^2\left(\frac{\omega}{2T}\right) S(\omega, k). \tag{6}$$

The dynamic structure factor is routinely measured in inelastic neutron-scattering experiments and thus provides a highly accessible measure of the multipartite entanglement of a system. In the zero-temperature limit the QFI Eq. (4) reduces to the variance of the operator $\hat{O}$,

$$F_Q = 4(\langle\hat{O}^2\rangle - \langle\hat{O}\rangle^2). \tag{7}$$

Another experimentally accessible entanglement monotone is the quantum variance [25]. The idea is that at finite temperature both thermal and quantum fluctuations contribute to the variance,

$$\langle\delta^2\hat{O}\rangle \equiv \langle\hat{O}^2\rangle - \langle\hat{O}\rangle^2, \tag{8}$$

so that we may write

$$\langle\delta^2\hat{O}\rangle = \langle\delta^2\hat{O}\rangle_Q + \langle\delta^2\hat{O}\rangle_T, \tag{9}$$

with the quantum fluctuations being some indicator of the extent to which a state may be entangled. In order to isolate the quantum component of the fluctuations we may use the fact that the thermal component of the fluctuations is simply given by the susceptibility. We therefore have

$$\langle\delta^2\hat{O}\rangle_Q = \langle\delta^2\hat{O}\rangle - \chi_{\hat{O}}k_BT. \tag{10}$$

It can be shown that the QV imposes both an upper and lower bound on the QFI [25,34],

$$4\langle\delta^2\hat{O}\rangle_Q \leqslant F_Q \leqslant 12\langle\delta^2\hat{O}\rangle_Q. \tag{11}$$

Additionally we can see that the total variance of the operator must be an upper bound to the QFI [16]. In Sec. III we compute these quantities and use them to assess the regime of validity of the single-mode approximated QFI. Both the QFI [19] and the QV [25] are thought to take a universal form at the quantum critical point. The exact scaling behavior of these quantities will ultimately be inherited from the operator in terms of which they are defined.

The work in the Supplemental Material of [19] derives the scaling exponents for the QFI density at both zero and finite temperature. We summarize their results here for convenience. For a review of scaling theory one can refer to [35]. Consider a rescaling of the lattice by an amount $\lambda$. The operator $\hat{O}$ will then rescale by some amount $\lambda^{-\Delta_\alpha}$. The QFI density will therefore scale as $\lambda^{d-2\Delta_\alpha}$. Thus, we can identify $\Delta_Q = d - 2\Delta_\alpha$ as the scaling dimension for the QFI density. This result holds in the finite temperature case as well. In order to demonstrate this we recall that the temperature and frequency both scale with the dynamical critical exponent $z$. By examining Eq. (6), we see that the argument of the hyperbolic tangent function is thus scale invariant. That leaves us with the scaling of the dynamical structure factor which scales in the same way as the correlation function, and thus the finite temperature QFI will also scale as $\Delta_Q = d - 2\Delta_\alpha$. For large but finite systems at low but nonzero temperatures we then expect [19]

$$f_Q(T, L) = \lambda^{\Delta_Q} h(\lambda^z T, \lambda/L), \tag{12}$$

where $L$ is the linear size of the system. If simulations are performed at low enough temperatures that the scaling with $T$ can be neglected, it then follows from finite-size scaling that

$$f_Q(L) \sim L^{\Delta_Q}. \tag{13}$$

### B. The single-mode approximation

We consider the first-principles definition of the structure factor for the spectrum of the Hermitian operator $\hat{O}$ [36]

$$S(\omega, k) = 2\pi \sum_{\lambda,\lambda'} p_\lambda |\langle\lambda'|\hat{O}|\lambda\rangle|^2 \delta(\omega + E_\lambda - E_{\lambda'}), \tag{14}$$

where $p_\lambda = e^{\beta E_\lambda}/\mathcal{Z}$. The structure factor is a function of $k$ through the definition of the $\hat{O}$. In the limit of $T \to 0$ it can be shown that Eq. (14) takes on the simpler form:

$$S(\omega, k) = \sum_{i,\lambda'} |\langle\lambda'|\hat{O}|0\rangle_i|^2 \delta(\omega + E_0 - E_{\lambda'}). \tag{15}$$

Here $|0\rangle$ is intended to represent the ground state. In general, the ground state may be degenerate. The summation index $i$ includes all states having the ground-state energy $E_0$. The content of the single-mode approximation is twofold. First we assume that only the first two energy levels are substantially populated. Second, we assume that transitions from the ground states to states at energies above the first excited state have negligible matrix elements compared with transitions from the ground-state manifold to the first excited state. That is to say,

$$S(\omega, k) = S_0(k)\delta\left(\omega - \omega_k^{(01)}\right) + \tilde{S}(k, \omega), \tag{16}$$

where $|S_0(k)| \gg |\int_{-\infty}^{\infty} \tilde{S}(\omega, k) d\omega|$, and $\omega_k^{(01)} := E_1 - E_0$. In other words, the bulk of the spectral weight is on the transition between the ground state and the first excited state. The $\tilde{S}(\omega, k)$ represents the spectral weight coming from states above the first excited state. Details of this approximation are derived in the Appendix.

In order to employ the single-mode approximation we need some way to determine the gap, $\omega_k^{(01)}$ (we henceforth drop the superscript and allow $\omega_k$ to denote the dispersion for the first excited state). It is clear that due to energy conservation $\text{supp}(\tilde{S}) = \{\omega : \omega_k < \omega_c < \omega\}$, where $\omega_c$ denotes the bottom of the continuous portion of the energy spectrum. In order to determine $\omega_k$ we multiply Eq. (16) by $\omega$ and integrate over all frequencies:

$$\frac{1}{\omega_k}\int_{-\infty}^{\infty} d\omega\, \omega S(\omega, k) = S_0(k) + \frac{1}{\omega_k}\int_{-\infty}^{\infty} d\omega\, \omega \tilde{S}(\omega, k). \tag{17}$$

In order to deal with the $\tilde{S}$, we note that

$$\frac{1}{\omega_k}\int_{-\infty}^{\infty} d\omega\, \omega \tilde{S}(\omega, k) \geqslant \int_{-\infty}^{\infty} d\omega\, \tilde{S}(\omega, k). \tag{18}$$

This assertion is made valid by the positive semidefinite nature of $\tilde{S}$. By substituting this inequality into Eq. (17) we see that the left-hand side is, by definition, the equal-time structure factor $S(k)$, giving

$$\frac{1}{S(k)}\int_{-\infty}^{\infty} d\omega\, \omega S(\omega, k) \geqslant \omega_k, \tag{19}$$

with

$$S^{\alpha\alpha}(k) \equiv \int S^{\alpha\alpha}(k, \omega) d\omega = \sum_r e^{-ikr} \langle S^\alpha(r) S^\alpha(0)\rangle. \tag{20}$$

We may use the following sum rule [37]:

$$\int_{-\infty}^{\infty} d\omega\, \omega S(\omega, k) = \pi \langle [\hat{O}^\dagger, [H, \hat{O}]]\rangle, \tag{21}$$

which applies to structure factors defined in terms of any operator, to evaluate this expression for the spin structure factor, which leaves the bound on $\omega_k$ as

$$\omega_k \leqslant \omega_{\text{SMA}}(k) := \pi \frac{\langle [\hat{O}^\dagger, [H, \hat{O}]]\rangle}{S(k)}, \tag{22}$$

where $\omega_{\text{SMA}}$ denotes the single-mode approximated dispersion. Here, $S(k)$ along with the different components of the commutator can be estimated relatively easily using quantum Monte Carlo methods from which $\omega_{\text{SMA}}(k)$ can then be obtained. Results are shown in Fig. 1(a) for the $S(k)$ from Fourier transforms of the ground-state correlation functions obtained from quantum Monte Carlo calculations. Figure 1(c) shows the resulting $\omega_{\text{SMA}}(k)$.

### C. The stochastic series expansion

The SSE framework is by now ubiquitous in condensed-matter theory. We here summarize only the specifics of what we measured, referring the reader to the literature for details on the SSE framework [28,29,38,39]. Static correlation functions are easily measured within the SSE by averaging the static correlation function over a number of configurations. More difficult is the measurement of quantities in imaginary time. For the case of the QV, we recall that the susceptibility in Eq. (10) is given by

$$\chi = \int_0^\beta d\tau \langle \hat{O}(\tau)\hat{O}(0)\rangle. \tag{23}$$

Following the prescription of [38] which involves expanding the imaginary time correlation function in the SSE framework

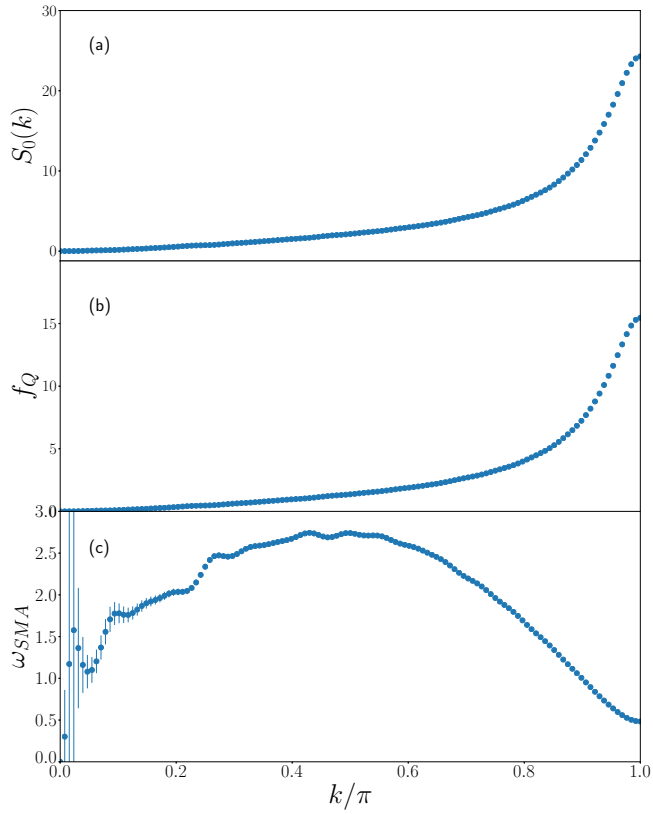


FIG. 1. (a) The equal-time structure factor for the isotropic $S = 1$ AFM model with $N = 256$, $\beta = 400$, exhibiting at peak at $k = \pi$. (b) The QFI density in the first Brillouin zone approaching zero at $k = 0$, and exhibiting a peak at $k = \pi$. (c) $\omega_k$ as obtained from the single-mode approximation. The characteristic gap of $0.41J$ at $k = \pi$ is clearly visible.

and exactly computing the integral, we arrive at

$$\chi = \left\langle \frac{\beta}{M(M+1)} \left( \sum_{p=0}^{M-1} o(p) \right)^2 + \frac{\beta}{(M+1)^2} \sum_{p=0}^{n} [o(p)]^2 \right\rangle, \tag{24}$$

where $M$ is the expansion order of the configuration being sampled, and $p$ is the propagation index within that expansion order. The total variance may also be measured directly from the SSE. Once the correlation functions are computed the appropriate transform may be applied to extract $S(k)$.

## III. RESULTS

We now turn to a discussion of our results for the QFI and multipartite entanglement in the $S = 1$ AFM Heisenberg model with uniaxial anisotropy,

$$\hat{H} = J \sum_i \left( \boldsymbol{S}_i \cdot \boldsymbol{S}_{i+1} + D\left(S_i^z\right)^2 \right). \tag{25}$$

This model has several appealing features to investigate multipartite entanglement. First, it possesses a symmetry-protected topological (SPT) phase with a gapped ground state in the isotropic region, with $\Delta \approx 0.41J$ [40,41]. This phase is characterized by the breaking of a hidden $\mathbb{Z}_2 \times \mathbb{Z}_2$ symmetry which establishes a long-range string order [42]. Second, the uniaxial anisotropy can drive two quantum phase transitions with critical points falling into two different universality classes. The phase diagram of this model has been extensively investigated in [43–45]. The first transition is from the SPT Haldane phase to a disordered phase with quasi-Néel ordering ($D_C^{HN} \approx -0.31$). The second transition is to a phase which is often called the "large-D phase" ($D_C^{HL} \approx 0.98$). This latter phase is essentially "empty" as the large uniaxial anisotropy forces each spin to have zero $S^z$ projection. The Haldane-Néel transition is in the universality class of the two-dimensional Ising model, while the Haldane-empty transition is in the Gaussian universality class. The excitation spectrum exactly at the isotropic point consists of a triplet state. This degeneracy is lifted away from the isotropic point into a heavier magnon with energy $\omega_k^{(\parallel)}$ and a lighter doublet with $\omega_k^{(\perp)}$. This notation is meant to evoke the fact that the heavier magnon is in the direction parallel to the uniaxial anisotropy, while the doublet corresponds to the transverse excitations. Most importantly, in a sizable region around $k = \pi$, as well as for $D \neq 0$, the dynamical structure factor is well approximated by a single mode.

We use SSE [28,30,39] techniques to numerically study the QFI within the single-mode approximation. All of the SSE simulations used in this section use on the order of $10^6$ Monte Carlo sweeps. The data for each observable is binned into groups of 1000 with the error bars estimated by taking the average variance over the bins.

In order to examine the quantum Fisher information we consider the operator, $S^z(\mathbf{k}) \equiv \hat{O} = \sum_r e^{ikr} \hat{S}_r^z$. The equal-time structure factor for this operator corresponds to the spectrum of spontaneous fluctuations in the longitudinal channel. Using Eq. (22) we may compute the bound on the dispersion for the heavy magnon to be [26]

$$\omega_{\mathrm{SMA}} = \frac{J\left(C_{xx}^{r,r+1} + C_{yy}^{r,r+1}\right)[1 - \cos(k)]}{S_0(k)}, \tag{26}$$

where $C_{\alpha\beta}^{ij} := \langle \hat{S}_i^\alpha \hat{S}_j^\beta \rangle$. For the case of periodic boundary conditions the ground state is not degenerate. We are here concerned with the singlet heavy magnon state. In this case $\eta_0 = \eta_1 = 1$ and thus, as per equation the leading thermal correction does not effect the QFI (see the Appendix for details). Since the single-mode approximation assumes these contributions to be small we ignore these thermal corrections. We may now apply the single-mode approximation to compute the QFI density,

$$f_Q(k) = 4 \tanh^2\left(\frac{\omega_k}{2T}\right) S_0(k) + \int_{-\infty}^{\infty} d\omega \, \tanh^2\left(\frac{\omega}{2T}\right) \tilde{S}(\omega, k), \tag{27}$$

where we shall neglect the last term arising from the continuum contribution. Since this last term corresponds to a positive contribution we would expect to obtain a lower bound on the QFI. We argue, however, that the dominant effect, particularly near the isotropic point, will come from the inequality, $\omega \leqslant \omega_{\mathrm{SMA}}$, Eq. (22). Hence, we believe that an overestimation of the QFI density is the more likely scenario. However, we expect this approximation to be rather good at low temperatures close to the isotropic point, $D = 0$, where

we then obtain the estimate for $f_Q$,

$$f_Q^{\mathrm{SMA}}(k) \sim 4\tanh^2\left(\frac{\omega_{\mathrm{SMA}}}{2T}\right)S_0(k). \tag{28}$$

We also note that the main $T$ dependence of $f_Q^{\mathrm{SMA}}(k)$ is now through the argument of the tanh. Up to this point Eq. (28) is completely model independent, relying only on ones ability to estimate the single mode. As per the results of Sec. II B, this may be said of any model with a gapped excitation spectrum. Near the critical point it is expected that the continuum will contribute more significantly to the behavior of the system especially at nonzero temperature, since the excitation gap closes. At the isotropic point the energy spectrum is gapped ($0.41J$). This means that the physics is dominated by the ground-state behavior until the temperature is raised sufficiently to excite higher energy states. This occurs when the temperature is roughly half the gap ($0.2J$). Because of this gap, the single-mode approximation is considerably more reliable at the isotropic point than at the critical point. With antiferromagnetic exchange, the equal-time structure factor peaks at the $k = \pi$ mode [Fig. 1(a)]. Thus the quantum Fisher information is maximal at the edge of the first Brillouin zone as shown in Fig. 1(b) where $f_Q^{\mathrm{SMA}}(k)$ is shown throughout the Brillouin zone. This corresponds to parametrizing the path through the space of density matrices using the staggered magnetization. At $k = 0$, $\hat{O}$ becomes the total magnetization which commutes with the Hamiltonian and thus cannot detect entanglement. As we approach $k = 0$ the single-mode approximation also becomes invalid since it is known that the well-defined single mode present around $k = \pi$ merges into the continuum. Fortunately the behavior of the single-mode approximation remains well controlled at the edge of the Brillouin zone where the QFI density detected by momentum space magnetization is maximal. In the following we therefore exclusively focus on $k = \pi$.

Let us first consider the finite temperature behavior of the entanglement at the isotropic point, $D = 0$. Using the QV we can make use of the established upper and lower bound on the QFI density. Combining this with Eq. (28) we then obtain

$$4\langle\delta^2\hat{O}\rangle_Q \leqslant F_Q \sim F_Q^{\mathrm{SMA}} \leqslant 12\langle\delta^2\hat{O}\rangle_Q. \tag{29}$$

On the other hand, the total variance is also an upper bound [6] on $f_Q$: $f_Q \leqslant 4\langle\delta^2\hat{O}\rangle/N$, where $\langle\delta^2\hat{O}\rangle$ refers to the total variance, Eq. (8). In Fig. 2 are shown results for $f_Q^{\mathrm{SMA}}(k = \pi)$ for a range of temperatures. In this regime the single-mode approximation should work quite well up until approximately half the gap. We see that, while the approximated QFI satisfies the upper bound given by the full variance, $\langle\delta^2\hat{O}\rangle$, for all temperatures up to the gap, $f_Q^{\mathrm{SMA}}$ breaks the upper bound given by the quantum variance at a temperature of approximately 0.275. We see that up until this point the approximated QFI density predicts the presence of multipartite entanglement well into this regime. If we use the quantum variance as a lower bound on $f_Q(k)$, then it predicts multipartite entanglement to temperatures approaching the gap. In Fig. 2 the shaded green region indicates the threshold to be exceeded for bipartite to be present and we note that both estimates of

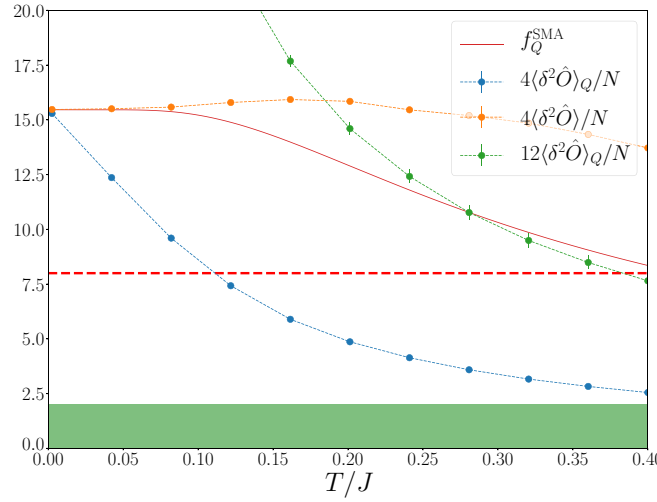


FIG. 2. Finite temperature behavior of the QFI density, $f_Q(k = \pi)$ and the quantum variance for temperatures up to the Haldane gap at the isotropic point, $D = 0$, for $N = 256$. $f_Q^{\mathrm{SMA}}$ is obtained from simulations at $\beta = 400$. Upper and lower bounds for $f_Q$ given by $4\langle\delta^2\hat{O}\rangle_Q/N$ (blue) and $12\langle\delta^2\hat{O}\rangle_Q/N$ (green) are shown along with the upper bound defined by the full variance, $4\langle\delta^2\hat{O}\rangle/N$. The green shaded region indicates the level that the $f_Q$ has to exceed to indicate the presence of *more than* bipartite entanglement. The dashed red line indicates the threshold for (8+1)-partite entanglement. Below that line and above the green region the system would be (4+1)-partite entangled.

$f_Q(k = \pi)$ indicate the presence of bipartite entanglement up to temperatures close to the gap.

We may now ask how the ground-state QFI density will behave as we approach the quantum critical point. Figure 3 shows the approximated QFI density indicated by the color intensity for a range of temperatures and $D$ values for a system size of 256 and $\beta = 400$ with periodic boundary conditions. We see that the QFI density is divergent at the quantum critical point, as expected from the behavior of $\hat{O}$. Figure 4 clearly shows the QFI density predicted by the single-mode approximation decays rapidly above the critical point, as the gap has now effectively closed. In this case the hard upper bounds given by the quantum variance are violated at relatively low temperatures. This is not surprising, as we expect the SMA to function only at the very lowest temperatures. Nonetheless, the approximated QFI remains below the bound given by the full variance. We see in this case that there is still persistent multipartite entanglement at finite temperatures above the quantum critical point.

The divergence of the entanglement at the critical point is seen by examining the QFI density for various system sizes. Figure 5 demonstrates the divergent scaling of both the QFI and the QV. Due to the fact that the Haldane-Néel transition is in the Ising universality class we can compute theoretically what the finite size scaling of the QFI density at the critical point must be. At low enough temperatures this is for finite systems given by Eq. (13). For the Ising universality class the critical exponent for the staggered magnetization is given by $\Delta_\alpha = 1/8$. This is confirmed in [44] using cluster expansion methods. This should give a QFI density scaling of $\Delta_Q = 3/4$. By examining even system sizes between $N = 64$ and

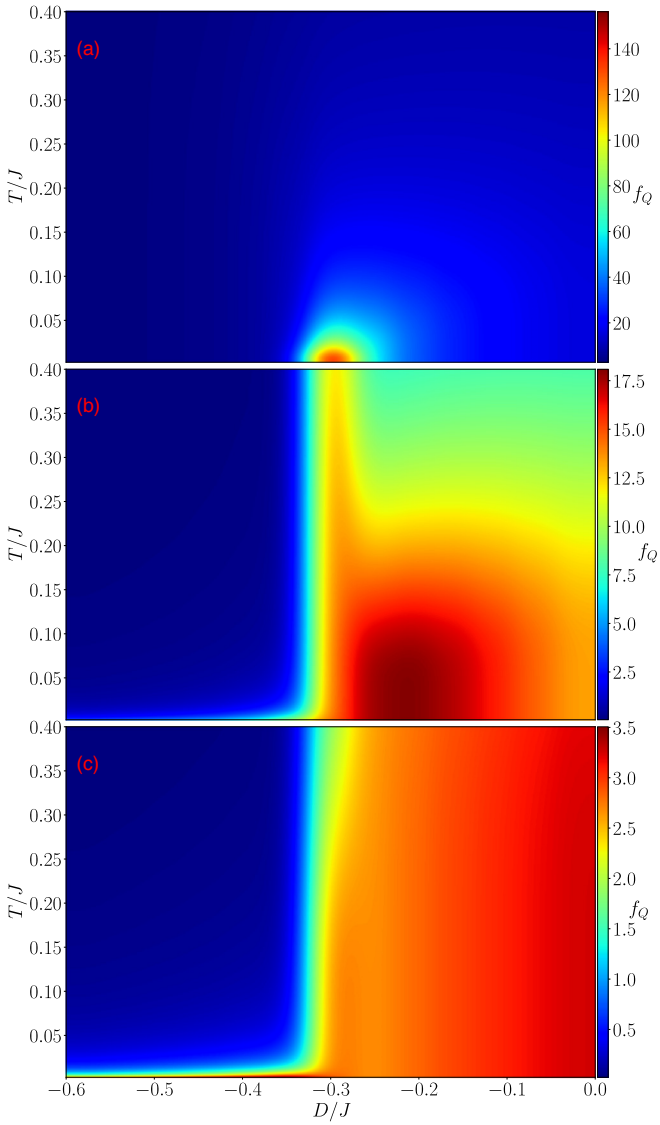


FIG. 3. QFI density detected for $\hat{O}(k) = \sum_r e^{ikr} S^z_r$ around the phase transition from the SPT Haldane phase to the disordered quasi-Néel phase for $N = 256$ for (a) $k = \pi$, (b) $k = 126\pi/128$, and (c) $k = 3\pi/4$. Obtained from SSE results ($\beta = 400$) and periodic boundary conditions. We note the diverging QFI density at the critical point, $D = -0.31$. In panel (c) we note that there appears to be persistent three-partite entanglement up to temperature on the order of the Haldane gap. Panel (c) shows the clear distinction in entanglement structure between the SPT phase for $D > -0.31$ and the disordered phase.

$N = 128$ at a $\beta = 400$ at a value of $D_C^{HN} = -0.31$ we estimate a QFI density scaling of $\Delta_Q = 0.7269(1)$. The error quoted here is associated with the quality of the linear regression. It does not account for systematic errors in the measurement of the QFI density. In order to estimate these systematic errors we examine subsets of four points and determine the maximum and minimum slopes that could be inferred from such four-point subset of the data. Using this we estimate a deviation of at least $\pm 0.06$. Thus the estimated scaling is $\Delta_Q = 0.73 \pm 0.06$. This estimate is consistent with the Ising universality class predicted for this transition.

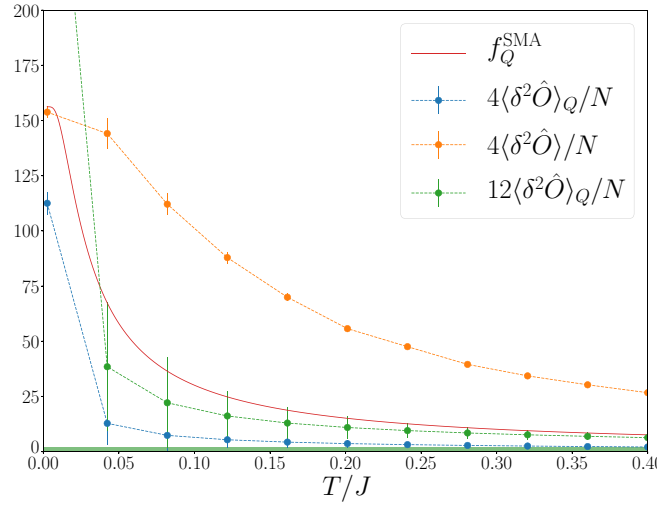


FIG. 4. Finite temperature QFI density and QV above the critical point for $N = 256$. $f_Q^{\mathrm{SMA}}$ is obtained from simulations at $\beta = 400$. Upper and lower bounds for $f_Q$ given by $4\langle\delta^2\hat{O}\rangle_Q/N$ (blue) and $12\langle\delta^2\hat{O}\rangle_Q/N$ (green), are shown along with the upper bound defined by the full variance, $4\langle\delta^2\hat{O}\rangle/N$. The green shaded region indicates the threshold $f_Q$ has to exceed for bipartite entanglement to be present.

## IV. CONCLUSIONS

Using the single-mode approximation we have shown that it is possible to obtain a quite simple estimate of the QFI density that should yield reliable results at temperatures well below the gap. We studied the $S = 1$ antiferromagnetic spin chain with uniaxial anisotropy within this approximation. The approximation yields results that are within rigorous upper and lower bounds at low temperatures where we expect the SMA to be a reasonable approximation. Clear signatures of

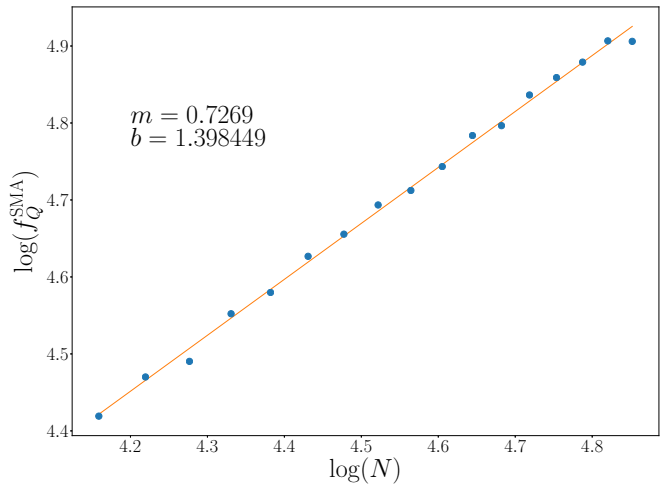


FIG. 5. Finite size scaling of the QFI density with system size for even system sizes between $N = 64$ and $N = 128$. Scaling was performed at $D = D_C = -0.31$ at $\beta = 400$ small enough that the system size would be the relevant perturbation to the scaling. The critical exponent with error due to the fit is found to be $\Delta_Q = 0.7269(1)$ with purely statistical error estimate.

multipartite entanglement were found at the isotropic point, $D = 0$, with the QFI density diverging when approaching the quantum critical point. When combined with the QV, the single-mode approximated QFI allows one to place both upper and lower bounds on the finite temperature entanglement of gapped systems. More precise techniques for calculating the QFI density at finite temperatures in strongly correlated systems would clearly be very desirable. Alternatively, sharper lower or upper bounds on the QFI density than we have discussed here would be very valuable.

We also note that the QFI has been linked to the canonical energy in gravitational physics [46] and can be expressed in terms of the relative entropy [47], developments which could potentially be exploited for more efficient numerical calculations of the QFI.

## ACKNOWLEDGMENTS

We would like to acknowledge Tomasso Roscilde for helpful discussions regarding the upper bound given by the QV and for alerting us to [34]. We acknowledge the support of the Natural Sciences and Engineering Research Council of Canada (NSERC). This work was supported in part by SHARCNET and Compute/Calcul Canada.

## APPENDIX: DETAILS OF THE SINGLE-MODE APPROXIMATION

We herein consider the details of the SMA and its leading order thermal corrections. Our aim is to show explicitly how one arrives at Eq. (16), and how the finite temperature corrections to this equation may be accounted for. Recall the definition of the structure factor,

$$S(\omega, k) = 2\pi \sum_{\lambda,\lambda'} p_y |\langle\lambda'|\hat{O}|\lambda\rangle|^2 \delta(\omega + E_\lambda - E_{\lambda'}). \quad \text{(A1)}$$

In the case where the system is in thermal equilibrium with a bath of inverse temperature $\beta$, the probabilities $p_\lambda$ are drawn from a Gibbs ensemble, $\hat{\rho} = \exp -\beta\hat{H}/\mathcal{Z}$, where $\mathcal{Z}$ is the partition function, $\mathcal{Z} = \mathrm{Tr}\exp -\beta\hat{H}$. For compactness, we denote the product of the matrix element amplitude and the delta function $\Gamma_{\lambda,\lambda'} \equiv |\langle\lambda'|\hat{O}|\lambda\rangle|^2\delta(\omega + E_\lambda - E_{\lambda'})$. In the following derivation we identify $E_0$ as the ground-state energy of the system, and $|0_i\rangle$ as the set of states in the ground-state manifold, with $\eta_\lambda$ being the number of states in the manifold with energy $E_\lambda$. Further, we denote the difference between two energy levels, $\lambda$ and $\lambda'$ as $\omega_{\lambda\lambda'} \equiv E_\lambda - E_{\lambda'}$. Let us expand Eq. (A1), and manipulate it so as to more easily take the zero temperature limit,

$$\begin{aligned} S(\omega, k) &= 2\pi \frac{\sum_{\lambda,\lambda'} e^{-\beta E_\lambda}\Gamma_{\lambda,\lambda'}}{\sum_\lambda \eta_\lambda e^{-\beta E_\lambda}} \\ &= 2\pi \frac{e^{-\beta E_0}\left(\sum_{i,\lambda'}\Gamma_{0_i,\lambda'} + \sum_{\lambda\neq 0_i,\lambda'} e^{-\beta\omega_{\lambda 0}}\Gamma_{\lambda,\lambda'}\right)}{e^{-\beta E_0}\left(\eta_0 + \sum_{\lambda\neq 0_i}\eta_\lambda e^{-\beta\omega_{\lambda 0}}\right)} \\ &= 2\pi \frac{\sum_{i,\lambda'}\Gamma_{0_i,\lambda'} + \sum_{\lambda\neq G_i,\lambda'} e^{-\beta\omega_{\lambda 0}}\Gamma_{\lambda,\lambda'}}{\eta_0 + \sum_{\lambda\neq 0_i}\eta_\lambda e^{-\beta\omega_{\lambda 0}}}. \end{aligned} \quad \text{(A2)}$$

We are now in a position to take the zero temperature limit of Eq. (A2). This is equivalent to the limit where $\beta$ goes to infinity. Clearly, $\omega_{\lambda 0}$ is strictly positive for the case where $|\lambda\rangle$ is not in the ground-state manifold. Thus when taking the zero temperature limit we find that the only remaining term is

$$S^{T=0}(\omega, k) = \frac{2\pi}{\eta_0}\sum_{i,\lambda'} |\langle 0_i|\hat{O}|\lambda'\rangle|^2\delta(\omega + E_0 - E_{\lambda'}). \quad \text{(A3)}$$

So far this has been exact. The single-mode approximation consists of assuming that the transition between the ground state and the first excited state constitutes the dominant transition in the system at zero temperature. More explicitly,

$$S^{T=0}(\omega, k) = 2\pi \frac{[S_0(k)\delta(\omega - \omega_{10}) + \tilde{S}(\omega, k)]}{\eta_0}, \quad \text{(A4)}$$

where

$$S_0(k) \equiv \sum_{i,j} |\langle 0_i|\hat{O}|1_j\rangle|^2, \quad \text{(A5)}$$

where $|1_j\rangle$ is the $j$th state in the energy manifold of the first excitation energy, and

$$\tilde{S}(\omega, k) \equiv \sum_{i,\lambda'}\Gamma_{0_i,\lambda'}. \quad \text{(A6)}$$

The single-mode approximation is then formally expressed by arguing that $|\langle 0_i|\hat{O}|1_j\rangle|^2 \gg |\langle 0_i|\hat{O}|\lambda\rangle|^2$, which means that Eq. (A4) becomes

$$S^{T=0}_{\mathrm{SMA}}(\omega, k) \approx 2\pi \frac{\sum_{i,j} |\langle 0_i|\hat{O}|1_j\rangle|^2\delta(\omega - \omega_{10})}{\eta_0}. \quad \text{(A7)}$$

At finite temperature it becomes possible for higher energy states to be occupied, and for transitions from these excited states to lower and higher energy states to make contributions to the spectral weight. We can make progress here by including the leading thermal correction and subsequently applying the same single-mode approximation argument. Consider the low-temperature structure factor which includes terms with the Boltzmann weight $\exp -\beta\omega_{10}$,

$$S^{T\ll 1}(\omega, k) = 2\pi \frac{\sum_{i,j} |\langle 0_i|\hat{O}|1_j\rangle|^2[\delta(\omega - \omega_{10}) + \delta(\omega + \omega_{10})e^{-\beta\omega_{10}}] + \sum_{i,\lambda}\Gamma_{0_i,\lambda} + \sum_{j,\lambda} e^{-\beta\omega_{\lambda 1}}\Gamma_{1_j,\lambda}}{\eta_0 + \eta_1 e^{-\beta\omega_{10}}}. \quad \text{(A8)}$$

We may now apply the same single-mode approximation to Eq. (A8) as we did the zero temperature, Eq. (A4), which results in

$$S^{T\ll 1}_{\mathrm{SMA}}(\omega, k) = 2\pi \frac{\sum_{i,j} |\langle 0_i|\hat{O}|1_j\rangle|^2[\delta(\omega - \omega_{10}) + \delta(\omega + \omega_{10})e^{-\beta\omega_{10}}]}{\eta_0 + \eta_1 e^{-\beta\omega_{10}}}. \quad \text{(A9)}$$

Substituting the above expression into the definition of the QFI and using the equal-time structure factor, $S(k)$, we are left with the following approximation:

$$f_Q^{\mathrm{SMA}} \approx 4 \tanh^2 \left(\frac{\omega_{10}}{2T}\right) S(k). \tag{A10}$$

The SMA is thought to be valid when a system exhibits a gapped excitation spectrum, at temperatures that are small enough relative to the energy gap that the system is unlikely to be found in an excited state. In the case of the Haldane model this occurs at approximately half the Haldane gap ($0.2J$), as can be seen in the work by Becker *et al.* [48], amongst other works.


[1] D. Petz and C. Sudár, J. Math. Phys. **37**, 2662 (1996).
[2] D. Petz, J. Phys. A: Math. Gen. **35**, 929 (2002).
[3] M. G. A. Paris, Int. J. Quantum. Inf. **07**, 125 (2009).
[4] G. Tóth, Phys. Rev. A **85**, 022322 (2012).
[5] G. Tóth and D. Petz, Phys. Rev. A **87**, 032324 (2013).
[6] G. Tóth and I. Apellaniz, J. Phys. A: Math. Theor. **47**, 424006 (2014).
[7] L. Pezzé and A. Smerzi, Phys. Rev. Lett. **102**, 100401 (2009).
[8] P. Hyllus, W. Laskowski, R. Krischek, C. Schwemmer, W. Wieczorek, H. Weinfurter, L. Pezzé, and A. Smerzi, Phys. Rev. A **85**, 022321 (2012).
[9] J. Eisert, M. Cramer, and M. B. Plenio, Rev. Mod. Phys. **82**, 277 (2010).
[10] N. Laflorencie, Phys. Rep. **646**, 1 (2016).
[11] M. Headrick, Phys. Rev. D **82**, 126010 (2010).
[12] R. Horodecki, P. Horodecki, M. Horodecki, and K. Horodecki, Rev. Mod. Phys. **81**, 865 (2009).
[13] V. Vedral, M. B. Plenio, M. A. Rippin, and P. L. Knight, Phys. Rev. Lett. **78**, 2275 (1997).
[14] L. Amico, R. Fazio, A. Osterloh, and V. Vedral, Rev. Mod. Phys. **80**, 517 (2008).
[15] M. B. Plenio and S. Virmani, Quant. Inf. Comput. **7**, 1 (2007).
[16] L. Pezzè, M. Gabbrielli, L. Lepori, and A. Smerzi, Phys. Rev. Lett. **119**, 250401 (2017).
[17] A. Rivas, S. F. Huelga, and M. B. Plenio, Rep. Prog. Phys. **77**, 094001 (2014).
[18] A. M. Kaufman, M. E. Tai, A. Lukin, M. Rispoli, R. Schittko, P. M. Preiss, and M. Greiner, Science **353**, 794 (2016).
[19] P. Hauke, L. Tagliacozzo, and P. Zoller, Nat. Phys. **12**, 778 (2016).
[20] W.-F. Liu, J. Ma, and X. Wang, J. Phys. A: Math. Theor. **46**, 045302 (2013).
[21] Q. Zheng, Y. Yao, and X.-W. Xu, Commun. Theor. Phys. **63**, 279 (2015).
[22] S.-S. Li, H.-G. Yi, and R.-H. Chen, Int. J. Theor. Phys. **52**, 1175 (2013).
[23] J. Ma and X. Wang, Phys. Rev. A **80**, 012318 (2009).
[24] C. Zhang, B. Yadin, Z.-B. Hou, H. Cao, B.-H. Liu, Y.-F. Huang, R. Maity, V. Vedral, C.-F. Li, G.-C. Guo *et al.*, Phys. Rev. A **96**, 042327 (2017).
[25] I. Frérot and T. Roscilde, Phys. Rev. B **94**, 075121 (2016).
[26] E. S. Sørensen and I. Affleck, Phys. Rev. B **49**, 15771 (1994).
[27] O. Golinelli, T. Jolicœur, and E. Sørensen, Eur. Phys. J. B **11**, 199 (1999).
[28] A. W. Sandvik and J. Kurkijärvi, Phys. Rev. B **43**, 5950 (1991).
[29] A. W. Sandvik, Phys. Rev. B **57**, 10287 (1998).
[30] O. F. Syljuåsen and A. W. Sandvik, Phys. Rev. E **66**, 046701 (2002).
[31] W. K. Wootters, Phys. Rev. D **23**, 357 (1981).
[32] S. L. Braunstein and C. M. Caves, Phys. Rev. Lett. **72**, 3439 (1994).
[33] M. Gessner and A. Smerzi, Phys. Rev. A **97**, 022109 (2018).
[34] I. Frérot and T. Roscilde, arXiv:1805.03140.
[35] J. Cardy, *Scaling and Renormalization in Statistical Physics* (Cambridge University Press, Cambridge, UK, 1996), Vol. 5.
[36] S. Lovesey, *Condensed Matter Physics: Dynamic Correlations*, Frontiers in Physics (Benjamin Cummings, San Francisco, 1980).
[37] P. Hohenberg and W. Brinkman, Phys. Rev. B **10**, 128 (1974).
[38] A. Dorneich and M. Troyer, Phys. Rev. E **64**, 066701 (2001).
[39] A. W. Sandvik, Phys. Rev. B **59**, R14157 (1999).
[40] F. D. M. Haldane, Phys. Rev. Lett. **50**, 1153 (1983).
[41] I. Affleck, Phys. Rev. B **41**, 6697 (1990).
[42] T. Kennedy and H. Tasaki, Phys. Rev. B **45**, 304 (1992).
[43] Z. Zhang, K. Wierschem, I. Yap, Y. Kato, C. D. Batista, and P. Sengupta, Phys. Rev. B **87**, 174405 (2013).
[44] A. F. Albuquerque, C. J. Hamer, and J. Oitmaa, Phys. Rev. B **79**, 054412 (2009).
[45] W. Chen, K. Hida, and B. C. Sanctuary, Phys. Rev. B **67**, 104401 (2003).
[46] N. Lashkari and M. Van Raamsdonk, J. High Energy Phys. 04 (2016) 153.
[47] M. van Raamsdonk, *New Frontiers in Fields and Strings: TASI 2015 Proceedings of the 2015 Theoretical Advanced Study Institute in Elementary Particle Physics* (World Scientific, 2017), pp. 297–351.
[48] J. Becker, T. Köhler, A. C. Tiegel, S. R. Manmana, S. Wessel, and A. Honecker, Phys. Rev. B **96**, 060403 (2017).